Systematic study of fusion suppression for tightly bound projectiles at above-barrier energies

M. Shariq Asnain,[1,*] Mohd. Shuaib,[1] Ishfaq Majeed,[1] Manoj Kumar Sharma,[2] Vijay R. Sharma,[3] Abhishek Yadav,[4] Devendra P. Singh,[5] Pushpendra P. Singh,[6] Sushil Kumar,[7] R. Kumar,[7] B. P. Singh,[1,†] and R. Prasad[1]

[1]*Accelerator Laboratory, Department of Physics, Aligarh Muslim University, Aligarh 202 002, Uttar Pradesh, India*
[2]*Department of Physics, Shri Varshney College, Aligarh 202 001, Uttar Pradesh, India*
[3]*Instituto de Fisica, Universidad Nacional Autonoma de Mexico, Mexico City 04510, Mexico*
[4]*Department of Physics, Faculty of Natural Sciences, Jamia Millia Islamia, New Delhi 110025, India*
[5]*Department of Physics, University of Petroleum and Energy Studies, Dehradun 248 007, Uttarakhand, India*
[6]*Department of Physics, Indian Institute of Technology, Ropar 140 001, Punjab, India*
[7]*Inter University Accelerator Centre, Aruna Asaf Ali Marg, New Delhi 110067, India*

(Received 19 November 2021; accepted 20 December 2021; published 10 January 2022)

The present work aims to explore the effects of projectile breakup on fusion cross section at energies near the Coulomb barrier to well above it. The complete fusion cross section for the strongly bound non-α-cluster projectile ^{14}N in interaction with a ^{181}Ta target was obtained by summing the experimentally measured channel-by-channel cross section data of evaporated residues. The obtained total fusion cross section was compared with the theoretical code CCFULL and the results were found to be consistent with each other. Further, the experimental fusion function data on ^{181}Ta target with ^{14}N projectile were deduced and compared with those obtained for other strongly bound projectiles, viz., ^{12,13}C, ^{16}O, and ^{19}F, in order to get some systematics in fusion reactions. The analysis of experimental fusion functions was performed within the framework of a benchmark curve called the universal fusion function (UFF). A suppression of about 5–25% with respect to UFF was observed for the presently studied systems at energies above the Coulomb barrier, indicating that the suppression is essentially due to the prompt breakup of the projectiles and is a strong function of breakup threshold of projectiles. The magnitude of such suppression was found to be lower for ^{14}N projectile as compared to other strongly bound projectiles. Moreover, an interesting exponential relation between the experimentally deduced suppression factor and the breakup threshold of the projectile was obtained.

DOI: 10.1103/PhysRevC.105.014609

I. INTRODUCTION

The study of heavy-ion (HI) induced fusion processes, in order to understand different mechanisms involved in these reactions, has been a topic of interest in nuclear physics. With varying projectile energies, the complex nature and behavior of projectile and target nuclei makes it possible to characterize the reaction mechanism and may help to study the possibility of producing superheavy elements (SHE) in the laboratory [1–5]. Recent studies on HI interactions indicate the presence of incomplete fusion (ICF) processes along with the complete fusion (CF) even at low energies ≈4–7 MeV/A [6–12]. In the case of CF, the target hugs the entire projectile with all the incoming partial waves of input angular momenta $\ell < \ell_{\rm crit}$, contributing to the formation of a highly excited composite system. In the case of ICF reactions, the projectile breaks up into fragment(s) and one of the fragment(s) fuses with the target nucleus, whereas the remnant continues to move in the beam direction without any interaction. In such cases, the fusion of the entire projectile with the target nucleus is hindered for angular momentum values $\ell > \ell_{\rm crit}$. Experimentally, the analysis of fusion processes in the case of HI reactions is rather delicate due to the competition of other reaction mechanisms such as transfer, breakup, preequilibrium reactions, etc. Further, the breakup and the preequilibrium emission may become important [13] at relatively higher energies and has attracted a great deal of interest in recent years [14,15]. In the literature, investigations carried out for HI fusion reactions suggest that the effective potential $V_{\rm eff}(r)$, which is the sum of nuclear, Coulomb and centrifugal potential, is sensitive around the nuclear surface region and is given as

$$V_{\rm eff}(r,\ell) = V_{\rm nucl}(r) + V_{\rm Coul}(r) + V_{\rm cent}(r,\ell), \qquad (1)$$

where the terms $V_{\rm nucl}(r)$, $V_{\rm Coul}(r)$, and $V_{\rm cent}(r,\ell)$ represents the attractive nuclear, repulsive Coulomb, and repulsive centrifugal potentials respectively. A typical variation of effective potential $V_{\rm eff}(r)$ with relative separation (r) between projectile and target nucleus for different angular momentum (ℓ) values is shown in Fig. 1. As can be seen from this figure, there is an attractive pocket for lower values of ℓ, which is called the fusion pocket, where the complete fusion of projectile and target nucleus takes place. However, for higher values of ℓ, this pocket starts vanishing and fusion does not occur. Hence, in order to provide sustainable angular momentum for fusion to occur, the projectile may break up into fragments and lead to the ICF process. The presence of ICF reactions in HI collisions at these energies has inspired an interest to

*asnainshariq@gmail.com
†bpsinghamu@gmail.com

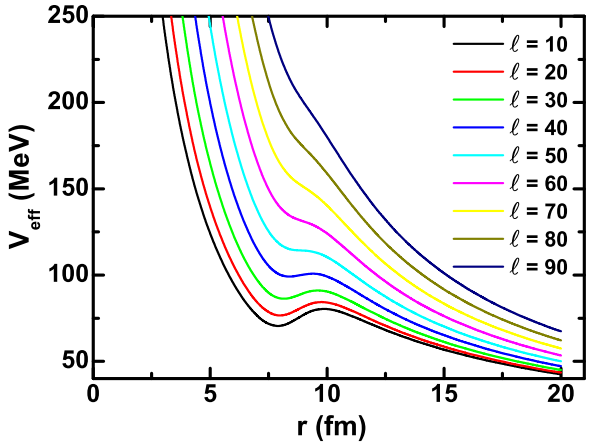

FIG. 1. A typical plot of effective potential V_{eff} as a function of relative separation r for different ℓ values. For details, see text.

study the effects of projectile breakup on fusion cross sections. Therefore, during the past several decades, both experimental and theoretical efforts have been made to investigate the effect of projectile breakup on fusion processes in HI collisions [16–18]. In order to perform a systematic study of breakup effects of projectile during the interaction process, it is necessary to follow proper data analysis procedure and eliminate the geometrical effects [19,20], if any, involved in fusion reactions. Such experimental data of different systems should only be compared with the theoretical predictions with and without coupling through breakup channels. Several data reduction procedures have been proposed to investigate the breakup effects near Coulomb barrier energies [21–24]; however, the widely used ones are used to compare the data with the predictions of coupled-channels (CC) calculations without considering the breakup channels [25–27] or with the predictions of the single barrier penetration model (SBPM) [28–31]. Gasques *et al.,* [30,32] after comparing the data with predictions of SBPM or CC calculations concluded that the CF suppression for reactions involving ^{6,7}Li and ^{10}B as projectiles is almost independent of target charge. On the other hand, Sargsyan *et al.* [33] investigated the influence of breakup effects on CF cross sections as a function of target charge and bombarding energy using the quantum diffusion approach. Gomes *et al.* [34] studied the influence of breakup effects on CF cross sections for ^{9}Be induced reactions by applying the universal fusion function (UFF) [19,23] approach. The aforesaid investigations could not observe a clear systematic behavior of CF suppression as a function of target charge. As such, there is a need to further investigate the systematic influence of projectile breakup on CF cross sections. The CF cross sections for many reactions involving weakly bound projectiles have been measured [27,35–38] where the suppression of CF cross section above the Coulomb barrier has been observed and is attributed to the breakup processes. However, for reactions involving strongly bound projectiles (especially non-α-cluster in nature), existing studies are limited. Hence, it is required to further explore the above for strongly bound projectiles as well. This may help in investigating the influence of breakup on CF cross section over a wide range of projectiles with different breakup threshold energies.

With this motivation, the analysis of experimental data for one of our recently measured ^{14}N + ^{181}Ta systems was performed within the framework of the universal fusion function (UFF) [19,23] approach. The present paper is organized as follows: A brief description of experimental details is given in Sec. II. Section III deals with the analysis and interpretation of UFF data. In Sec. IV a brief summary of the presently investigated system is presented.

II. EXPERIMENTAL DETAILS

In order to investigate the influence of projectile breakup, a program of measuring fusion cross section for various projectile-target combinations was undertaken. In the present experiments the interaction of ^{14}N with ^{181}Ta was performed using the Pelletron ion-beam facility of the Inter University Accelerator Centre (IUAC), New Delhi, India. The excitation functions (EF) for a large number of residues populated via CF and/or ICF processes were measured. Spectroscopically pure thin ^{181}Ta targets and aluminium catcher/energy-degrader foils were prepared by using the rolling technique. The thickness of each target was measured for precision by the α-transmission method. Three stacks each consisting of four target-catcher foil assemblies were irradiated separately at energies 87.07 ± 0.93, 85.17 ± 0.83, and 83.05 ± 0.95 MeV with a beam current of 4–5 p nA. The cross sections for various reaction residues were measured at twelve different energies ranging from ≈65 to 88 MeV to cover a broad range of EFs. The irradiations were carried out in the General Purpose Scattering Chamber (GPSC), which has an in-vacuum transfer facility (ITF). The activities induced in each sample were recorded several times using a high-purity germanium (HPGe) detector (100 cm^3 active volume) coupled to a computer-aided measurement and control (CAMAC) based data acquisition system. The resolution of the HPGe detector was 1.2 keV for the 1.33 MeV γ-ray of ^{60}Co. The energy and efficiency calibrations were done by using the standard γ sources, viz., ^{22}Na, ^{60}Co, ^{133}Ba, and ^{152}Eu. The calibration was checked several times during the experiments and dead time corrections were also made.

III. ANALYSIS AND INTERPRETATION OF DATA

A. Calculations with the code CCFULL

The channel-by-channel experimental cross section data of evaporation residues populated via xn/pxn channels, viz., ^{192}Hg($3n$), ^{191}Hg($4n$), ^{190}Hg($5n$), ^{189}Hg($6n$), ^{191}Au($p3n$), ^{190}Au($p4n$), and ^{189}Au($p5n$), were measured and compared with the predictions of theoretical model code PACE4 [39] over a wide range of energy. The cross sections for the $3n$, $4n$, $5n$, and $6n$ channels were found to be agree well with the statistical model predictions based on the CN model. However, in case of $p3n$, $p4n$, and $p5n$ channels, the contribution from the higher charge precursor decay was separated out for comparison with the predictions of PACE4. After separating the precursor contribution, the EFs for these residues agreed well with the theoretical predictions. These reaction residues were

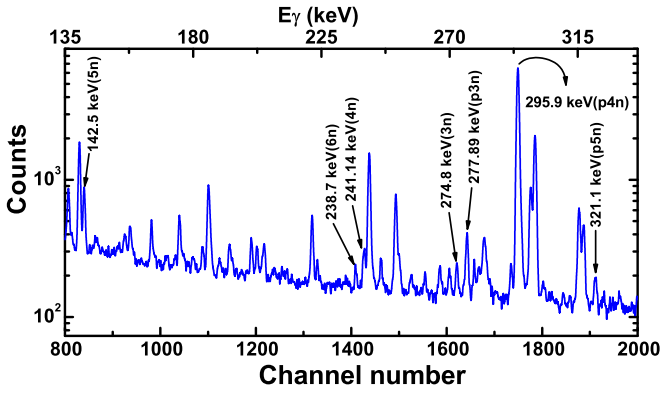

FIG. 2. A typical γ-ray spectrum of the $^{14}\mathrm{N}+^{181}\mathrm{Ta}$ system for all CF channels at 85.17 ± 0.83 MeV.

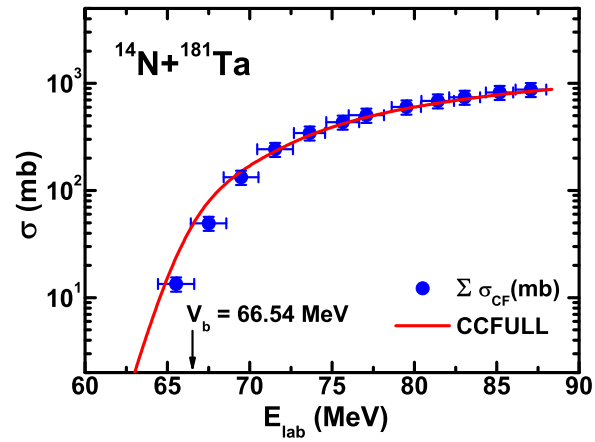

FIG. 3. The experimentally measured total complete fusion cross section $\sum \sigma_{CF}$ is plotted as a function of incident projectile energy. The red solid line denotes the theoretical fusion cross section calculated by using the code CCFULL.

identified by their characteristic γ rays from the recorded γ ray spectrum. As a representative case, the relevant portion of the γ-ray spectrum of the $^{14}\mathrm{N}+^{181}\mathrm{Ta}$ system recorded at 85.17 ± 0.83 MeV is shown in Fig. 2 and the γ peaks of the residues populated via CF channels are labeled by γ-ray energies as well. Further, the identification of these populated residues was also confirmed by measuring their half-lives using decay curve analysis.

Fusion reactions at energies above the Coulomb barrier have been well studied. Extensive experimental and theoretical studies have revealed that fusion reactions at energies near and below the barrier are strongly influenced by the coupling between the relative motion of the colliding nuclei [40,41]. In order to address the coupling effects between the relative motion of colliding nuclei and intrinsic degrees of freedom, the standard way is to solve the coupled-channels equations including all the relative channels. In order to study the above effects, a FORTRAN 77 based program CCFULL [42], which includes the couplings to all channels, was used to determine the fusion cross section. The coupled-channels differential equation is given by [42,43]

$$\left[\frac{-\hbar^2}{2\mu}\frac{d^2}{dr^2} + \frac{J(J+1)\hbar^2}{2\mu r^2} + V_N^{(0)}(r) + \frac{Z_P Z_T e^2}{r} + \epsilon_n - E\right] \times \psi_n(r) + \sum_m V_{nm}(r)\psi_m(r) = 0, \quad (2)$$

where r is the radial component of the coordinate of the relative motion, μ is the reduced mass, E is the bombarding energy in the center-of-mass frame, and ϵ_n is excitation energy of the nth channel. V_{nm} are the matrix elements of the coupling Hamiltonian and $V_N^{(0)}$ is the nuclear potential in the entrance channel. The coupled-channels equations can be solved by imposing boundary conditions. The total fusion cross section ($\sum \sigma_{CF}$) was obtained for the $^{14}\mathrm{N}+^{181}\mathrm{Ta}$ system from the sum of experimentally measured cross section values for various fusion channels and compared with the predictions of coupled-channels calculations done using the code CCFULL [42], as shown in Fig. 3. As can be seen from this figure, the experimental fusion cross section data match well with the predictions of the code CCFULL over the entire range of energy, which strengthens and justifies the validity of our measurements. In the coupled-channels (CC) formalism, the Wood-Saxon (WS) potential, which is a deep attractive potential, is used as a real nuclear potential and its depth (V_o) is chosen to reproduce the experimental cross section. The values of various parameters like V_o, r_o, and a_o used in this code to calculate fusion cross section are taken to be 61.4 MeV, 1.7 fm, and 0.63 fm respectively for the $^{14}\mathrm{N}+^{181}\mathrm{Ta}$ system. For these values of parameters, the theoretically calculated fusion cross section data agrees well with the experimentally measured fusion cross section data. It needs to be pointed out here that the above calculations do not consider couplings to unbound or continuum states. As such, the theoretical fusion cross sections were calculated without taking into account the contribution from breakup channels. The coupled-channels calculations are found to explain the fusion cross section data, in general, at above-barrier energies reasonably well; however, the inelastic excitations and transfer may not be accounted for simultaneously. The continuum-discretized coupled-channels (CDCC) calculations [44–47] may handle breakup and fusion reactions in a coherent manner, especially for the loosely bound projectiles [45,48–50]. However, the strongly bound $^{14}\mathrm{N}$ beam, employed in the present work, may be considered as an inert projectile that makes it easier to use the inclusive data provided by the activation method to analyze the results of presently measured cross section data within the framework of the universal fusion function (UFF) approach, described in the following sections. It may be mentioned that, in order to obtain a systematic analysis, the fusion cross section data needs to be compared for many projectile-target combinations, which needs a systematic data reduction procedure as discussed in the following section. This may also help us to get significant information regarding the effects of breakup probability on the fusion cross section data.

B. Reduction procedures and calculation of suppression factor

1. Comparison of fusion data

In the present work, the measured fusion cross section data for the $^{14}\mathrm{N}+^{181}\mathrm{Ta}$ system were compared with the

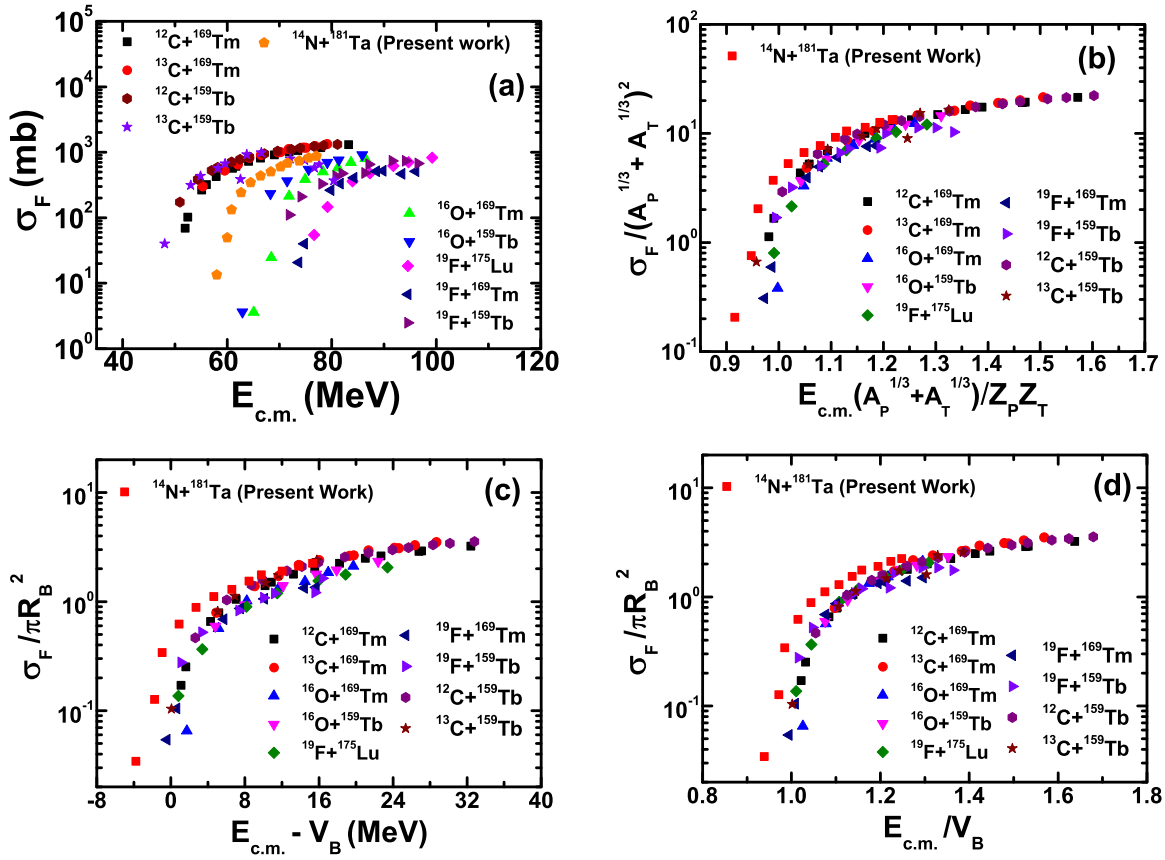

FIG. 4. Comparison of fusion cross section data for strongly bound projectiles. In (a) the data are compared directly while in (b), (c), and (d) the data are reduced by using different prescriptions. (For details, see text.)

corresponding data for the systems $^{12}C+^{169}Tm$, $^{12}C+^{159}Tb$, $^{13}C+^{169}Tm$, $^{13}C+^{159}Tb$, $^{16}O+^{169}Tm$, $^{16}O+^{159}Tb$, $^{19}F+^{169}Tm$, $^{19}F+^{159}Tb$, and $^{19}F+^{175}Lu$. As can be seen, these systems have the target nucleus in the mass number region from $A = 159$ to $A = 181$ and involving beams of $^{12,13}C$, ^{14}N, ^{16}O, and ^{19}F. This comparison is shown in Fig. 4(a). As can be seen from this figure, the fusion cross section data for the above mentioned projectile-target combinations when plotted as a function of center-of-mass energy are not in order, and no conclusion could be drawn with such a comparison of data. The observed scattered data for various systems may be due to geometrical effects. In order to wash out the geometrical effects, the fusion cross section may be normalized with respect to the geometrical parameters and the incident projectile energy with respect to the barrier height. The barrier height is calculated as $V_b = \frac{Z_P Z_T e^2}{4\pi\epsilon_o R_b}$ where Z_P and Z_T are the atomic numbers of projectile and target nucleus, respectively, and the barrier radius is approximated by $R_b = r_o(A_P^{1/3} + A_T^{1/3})$, where A_P and A_T are the mass numbers of projectile and target nucleus respectively. Since the different systems have different barrier heights, different values of barrier radius are associated. Hence, cross section may be normalized by the barrier radius while the center-of-mass energy may be normalized by the Coulomb factor ($Z_P Z_T$).

Such normalized values of cross section and energy plotted using the above procedures are shown in Fig. 4(b) for the presently studied system along with several other systems as already mentioned. It may be observed from this figure that some of the effects due to different sizes and Coulomb factor seem to be washed out as compared to Fig. 4(a), but not completely. Hence, in order to remove these effects completely, some other procedure may be adopted. The fusion cross section may also be influenced by geometrical cross section due to different sizes of target nuclei while the effective energy av ailable for the reaction is over the Coulomb barrier (V_b). In order to overcome the above, the fusion cross sections normalized with πR_B^2 are plotted with center-of-mass energy above the Coulomb barrier and normalized with V_b,in Figs. 4(c) and 4(d) respectively. As can be seen from these figures, the data for different systems now seem to be in good agreement with respect to each other. It may be remarked that these reductions still depend on the system used. However, minor deviations observed still need to be looked into and it is desirable to compare the data within some universal approach, as discussed below.

2. The universal fusion function

In order to obtain a systematic behavior of fusion cross section data in HI collisions, it may be better to use a standard procedure for reducing the fusion cross section data to eliminate the geometrical and static effects due to the potential acting between the interacting nuclei. In view of the above, a method suggested by Canto *et al.* [19,23] seems to be

TABLE I. List of different parameters used to calculate the experimental fusion function for various systems.

System	V_b (MeV)	R_b (fm)	$\hbar\omega$ (MeV)	$Z_P Z_T$	Ref.
$^{12}C+^{169}Tm$	50.83	10.99	4.5	414	[53]
$^{12}C+^{159}Tb$	48.3	10.88	4.4	390	[6]
$^{13}C+^{169}Tm$	50.44	11.08	4.3	414	[54]
$^{13}C+^{159}Tb$	47.97	10.97	4.2	390	[7]
$^{16}O+^{169}Tm$	66.7	11.16	4.37	552	[55]
$^{16}O+^{159}Tb$	63.47	11.04	4.34	520	[56]
$^{14}N+^{181}Ta$	61.77	11.27	4.36	511	[a]
$^{19}F+^{169}Tm$	74.12	11.29	4.24	621	[8]
$^{19}F+^{159}Tb$	70.78	11.14	4.17	585	[9]
$^{19}F+^{175}Lu$	75.83	11.36	4.23	639	[10]

[a]Effective lifetime not corrected for feedingPresent work.

appropriate and is adopted in the present work for normalizing the fusion cross section. In this approach, the fusion cross section (σ_F) is converted into a dimensionless quantity referred to as the fusion function $F(x)$ and the incident energy as a dimensionless variable x. A realistic potential is not only characterized by barrier height but also by its radius as well as curvature, and these values vary from system to system. The barrier curvature ($\hbar\omega$) influences the tunneling probability and is significantly important at lower energies. Both the dimensionless fusion function $F(x)$ and the variable x are deduced to account for the effects due to the above parameters as

$$F(x) = \frac{2E_{c.m.}}{\hbar\omega R_b^2}\sigma_F, \tag{3}$$

$$x = \frac{(E_{c.m.} - V_b)}{\hbar\omega}; \tag{4}$$

here, $E_{c.m.}$ is the collision energy in the center-of-mass frame, σ_F is the fusion cross section, and $\hbar\omega$, R_b, and V_b are the barrier curvature, barrier radius, and barrier height respectively. In the present work, the barrier parameters like $\hbar\omega$, R_b, and V_b are taken from the NRV code [51] and are given in Table I for various projectile-target combinations. The last column of this table gives references from where the experimental data are taken. The experimental fusion function $F(x)$ values are deduced from the measured cross sections and the corresponding theoretical values are obtained from the barrier parameters using Eq. (3). The reduction procedure given by Eqs. (3) and (4) was formulated by Wong [52] for the fusion cross section as

$$\sigma_F^W = \frac{R_b^2\hbar\omega}{2E_{c.m.}} \ln\left[1 + \exp\left(\frac{2\pi(E_{c.m.} - V_b)}{\hbar\omega}\right)\right]. \tag{5}$$

Replacing σ_F with σ_F^W from the above in Eq. (3), the fusion function $F(x)$ educes to another dimensionless function,

$$F_o(x) = \ln[1 + \exp(2\pi x)]. \tag{6}$$

The above relation is referred as the universal fusion function (UFF) [22] or $F_o(x)$ is a general function of a dimensionless variable x and does not depend upon the system properties. For $x > 1$, $F_o(x) \approx 2\pi x$. In the simple approach, at energies larger than Coulomb barrier, fusion cross section are calculated as

$$\sigma_F = \pi R_b^2(E_{c.m.} - V_b)/E_{c.m.}. \tag{7}$$

In the above expression, the fusion cross section is independent of width of the barrier and can simply be described as absorption of the incident flux by the nucleus representing a black disk of radius R_b. The reduction in CF flux may be understood as the partial fusion associated with the unfused fragment of the projectile not being confined within the black disk. As a result, a component of cross section due to incomplete fusion of projectile may reduce the experimental fusion cross section data. The reduction in fusion cross section may be investigated by comparing the data of different systems with those obtained from the UFF analysis. The lowering of experimental data with respect to the UFF may be attributed to the reduction in CF flux as a result of breakup and/or partial fusion of the projectile.

During the past few decades, CF cross section data for several reactions involving weakly bound projectiles have been measured [27,42–45] and suppression of CF cross section with respect to total fusion cross section above the barrier has been observed. Moreover, a significant contribution from ICF processes for reactions involving strongly bound projectiles has also been observed [6–10]. In order to investigate the effect of projectile breakup in the case of strongly bound projectiles as well, in the present work, the experimental fusion function data of a non-α-cluster beam ^{14}N on the target ^{181}Ta are presented and compared with the deduced fusion function for the systems, viz., $^{12}C+^{169}Tm$, $^{12}C+^{159}Tb$, $^{13}C+^{169}Tm$, $^{13}C+^{159}Tb$, $^{16}O+^{169}Tm$, $^{16}O+^{159}Tb$, $^{19}F+^{169}Tm$, $^{19}F+^{159}Tb$, and $^{19}F+^{175}Lu$. The deduced UFF have been analyzed within the framework of Wong's formations [52] and are plotted as shown in Figs. 5(a)–5(d) and 6. The solid black line in these figures represents the UFF obtained by Eq. (6) and the colored dashed line represents the best fitting to the experimental fusion function data. As may be seen, the experimental fusion functions for all the cases are found to be suppressed with respect to the UFF line indicating that some part of the incident flux has been reduced which may be attributed due to partial fusion as a result of breakup of the projectiles. It may be observed that the CF data are most suppressed for ^{19}F and least for ^{14}N projectile. An attempt has been made to explain the degree of suppression on the basis of breakup threshold energy ($E_{B.U.}$) of projectiles. The $E_{B.U.}$ of ^{19}F is 4.01 MeV, hence it is the least tightly bound projectile among all these, and ^{14}N is the most tightly bound projectile among all these, with a value of $E_{B.U.}$ equal to 11.62 MeV. The experimental fusion function for the CF data is found to be least suppressed for the most strongly bound projectile. Moreover, it can also be concluded from Figs. 5(a)–5(d) that the experimental fusion functions for the reactions induced by the same projectile are close to each other, which implies that the CF suppression is independent of the target charge. For the sake of completeness, the experimental fusion functions for all these systems are also shown together along with UFF in Fig. 7. The red and blue color dotted lines represents the range of suppression of CF cross section data and are obtained by multiplying the UFF with 0.95 and 0.76 respectively. It has

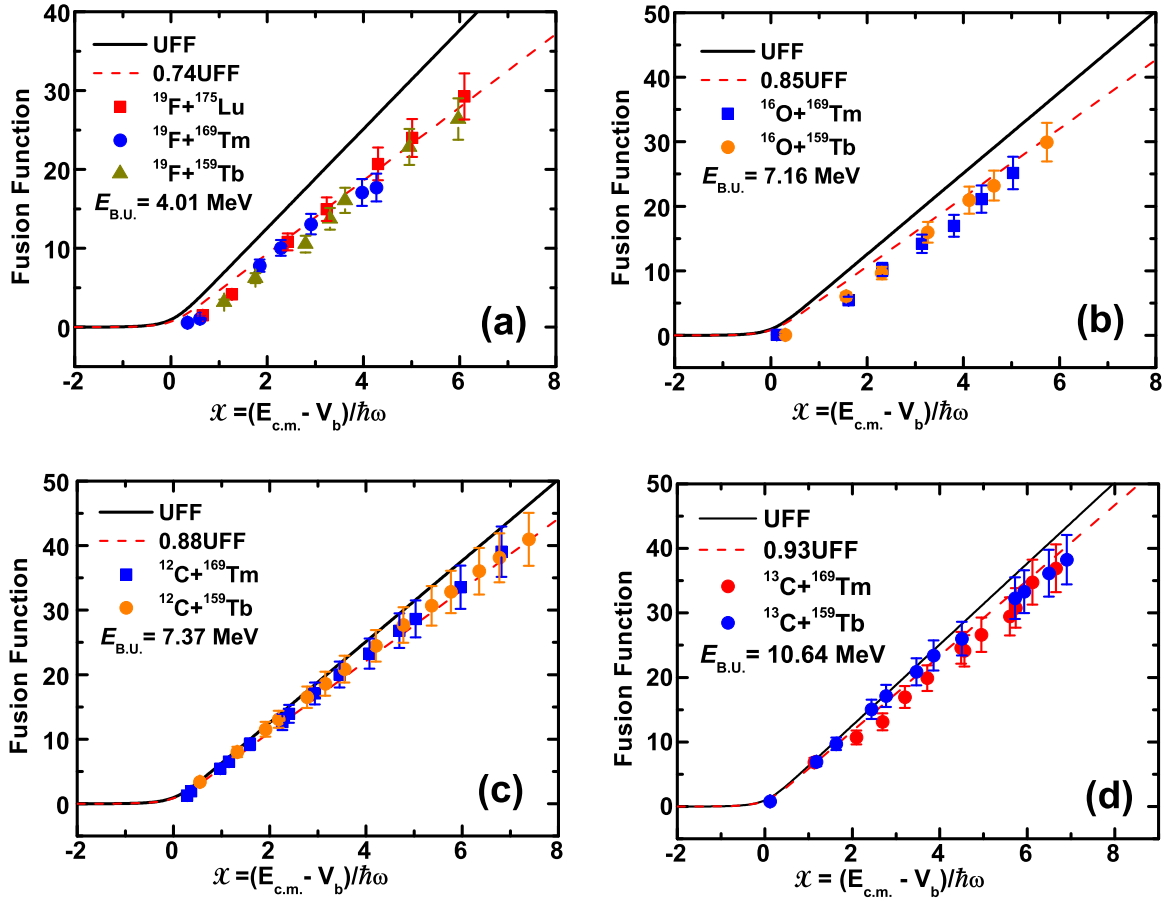

FIG. 5. The experimental fusion functions plotted separately for (a) ^{19}F projectile, (b) ^{16}O projectile, (c) ^{12}C projectile, (d) ^{13}C projectile, on different targets. The black solid line represents the UFF.

been found that there is a suppression of about 5–25% in CF data with respect to the UFF for the projectiles under study.

Further, the above analysis suggests that the suppression seems to be sensitive to the breakup threshold energy of the projectile. It has been observed from these figures that if the breakup threshold of the projectile is higher, the suppression is lower. As can be seen from the Fig. 6, the suppression with respect to UFF is found to be lowest for the ^{14}N projectile as compared to all the other projectilesm which is related to the fact that the breakup threshold of ^{14}N is highest ($E_{B.U.}$ = 11.62 MeV) among all these projectiles. In order to correlate the suppression with breakup threshold energy, the following

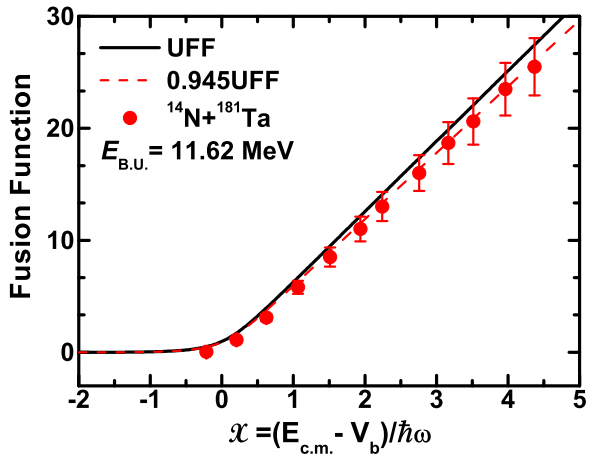

FIG. 6. The experimental fusion function for the ^{14}N + ^{181}Ta system. The black solid line represents the UFF.

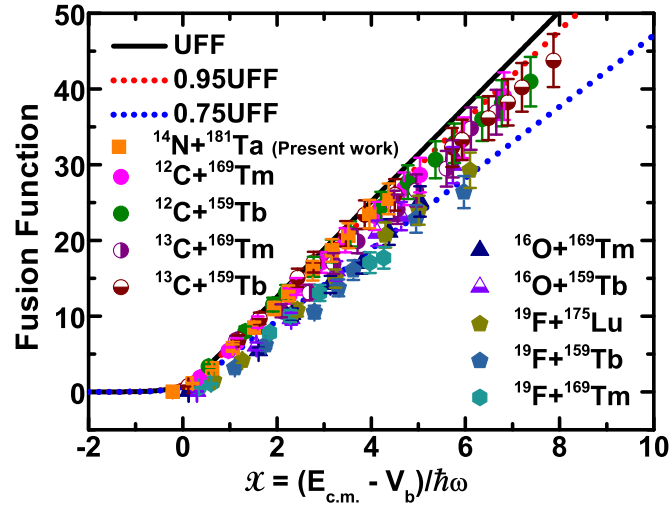

FIG. 7. The experimental fusion function for strongly bound projectiles on different target nuclei. The black solid line denotes the UFF. (For more details, see text.)

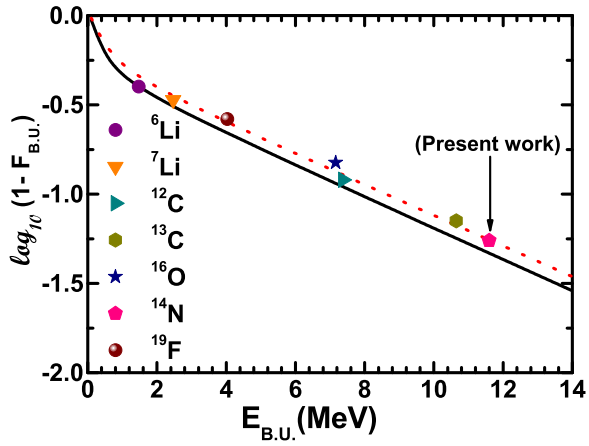

FIG. 8. The deduced suppression factors for various projectiles are plotted as a function of their breakup threshold energy. The black solid line represents the empirical relation given by Eq. (9) and red dotted line is given by Eq. (10).

empirical relation [57] may be used:

$$\log_{10}(1-F_{B.U.}) = -a\exp(-b/E_{B.U.}) - cE_{B.U.} \quad (8)$$

where a, b, and c are the fitting parameters and $E_{B.U.}$ is the breakup threshold energy of the projectile in MeV. $F_{B.U.}$ is the suppression factor obtained from the ratio of the experimental fusion function and $F_o(x)$ given by Eq. (6).

The values of the parameters a, b, and c suggested by Wang *et al.* are $a = 0.33$, $b = 0.29$ MeV, and $c = 0.087$ MeV^{-1}. As a result, Eq. (8) takes the form

$$\log_{10}(1-F_{B.U.}) = -0.33\exp(-0.29/E_{B.U.}) - 0.087E_{B.U.} \quad (9)$$

The suppression factor $F_{B.U.}$ for the present work using ^{14}N projectile was obtained by fitting the experimental fusion function data in Fig. 6 by multiplying the UFF with 0.945. A variation of $F_{B.U.}$ for various projectiles as a function of their respective breakup threshold energy is shown in Fig. 8. The black solid line in this figure represents the variation in suppression as per Eq. (9). It can be observed from this figure that the experimental data are not in very good agreement with the empirical equation [Eq. (9)] given by Wang *et al.* As such, the constants a, b, and c in Eq. (8) were varied as $a = 0.28$, $b = 0.39$ MeV, and $c = 0.085$ MeV^{-1}. Using these values of parameters, Eq. (8) becomes

$$\log_{10}(1-F_{B.U.}) = -0.28\exp(-0.39/E_{B.U.}) - 0.085E_{B.U.}. \quad (10)$$

A plot of the above equation is shown by the red dotted line in Fig. 8. It may be observed that the data points in Fig. 8 are found to be in good agreement with the empirical relation given by Eq. (10) rather than Eq. (9) given in Ref. [57]. Further, the trend is the same for both equations. The values of $\log_{10}(1-F_{B.U.})$ obtained from Eq. (10) by fitting the experimental data for different projectile-target combinations are shown in Table II. The analytical relation also suggests that effect of projectile breakup on fusion cross section is a breakup threshold energy effect.

TABLE II. The table shows the suppression factor obtained from the empirical formula (9) and by fitting the experimental fusion function data for different projectiles. The second column of this table shows the breakup threshold energy of the projectiles.

Projectile	$E_{B.U.}$ (MeV)	$\log_{10}(1-F_{B.U.})$ [Eq. (10)]	$F_{B.U.}$ (fit)	$\log_{10}(1-F_{B.U.})$ (fit)	Target
^{12}C	7.367	−0.89	0.88	−0.95	^{169}Tm
					^{159}Tb
^{13}C	10.648	−1.17	0.93	−1.15	^{169}Tm
					^{159}Tb
^{16}O	7.161	−0.87	0.85	−0.824	^{169}Tm
					^{159}Tb
^{14}N	11.62	−1.25	0.945	−1.26	^{181}Ta
^{19}F	4.014	−0.59	0.74	−0.58	^{169}Tm
					^{159}Tb
					^{175}Lu

IV. SUMMARY

In the present work, an attempt has been made to see the breakup effects of the strongly bound non-α-cluster projectile ^{14}N on fusion cross section at energies above the Coulomb barrier. The experimentally deduced total complete fusion cross section was compared and found to be in good agreement with the predictions of the theoretical code CCFULL over a wide range of energy. Moreover, the fusion cross section data for other systems involving strongly bound projectiles were compared with each other. Several reduction procedures were adopted in order to wash out the geometrical effects affecting the fusion data. Also, with the help of the experimentally deduced total complete fusion cross section, the experimental fusion function was deduced and compared within the framework of a benchmark curve called the universal fusion function. It was observed that the experimental fusion function for ^{14}N is ≈5% below the UFF. Along with the presently studied ^{14}N + ^{181}Ta system, the experimental fusion functions for various other systems were also deduced and compared with the theoretically calculated values of UFF. A significant suppression of about 5–25% in CF cross section was observed, which clearly suggests that the suppression is due to the prompt breakup of the projectiles. The CF suppression for reactions involving the same projectile was found to be independent of target charge. With the help of the experimental fusion function, the suppression factors for different projectiles were also deduced and a strong correlation between the breakup threshold of the projectile and the suppression was observed. The systematics developed by Wang *et al.* was modified by changing the fitting parameters, confirming that projectile breakup on fusion is a threshold energy effect.

In order to have a better understanding and to have a more clear and conclusive picture of the effects of projectile breakup on fusion cross section, theoretical studies in this direction along with more and more experimental data, especially for non-α-cluster projectiles, are required. New experimental data may help in developing universal systematics at energies ≈4–7 MeV/nucleon.

ACKNOWLEDGMENTS

The authors thank the Director, IUAC, New Delhi, India and the Chairperson, Department of Physics, Aligarh Muslim University, Aligarh (U.P.), India for providing all the necessary facilities to carry out this work. M.S.A. and B.P.S. thank the DST-SERB for providing financial support under Project No. CRG/2020/000136.

[1] Yu. Ts. Oganessian, A. V. Yeremin, A. G. Popeko, S. L. Bogomolov, G. V. Buklanov, M. L. Chelnokov, V. I. Chepigin, B. N. Gikal, V. A. Gorshkov, G. G. Gulbekian, M. G. Itkis, A. P. Kabachenko, A. Yu. Lavrentev, O. N. Malyshev, J. Rohac, and R. N. Sagaidak, Nature (London) **400**, 242 (1999).
[2] R. Smolanczuk, Phys. Rev. C **59**, 2634 (1999).
[3] S. Hofmann, D. Ackermann, S. Antalic, H. G. Burkhard, V. F. Comas, R. Dressler, Z. Gan, S. Heinz, J. A. Heredia, F. P. Heßberger, J. Khuyagbaatar, B. Kindler, I. Kojouharov, P. Kuusiniemi, M. Leino, B. Lommel, R. Mann,G. Münzenberg, K. Nishio, A. G. Popeko, S. Saro, H. J. Schött, B. Streicher *et al.*, Eur. Phys. J. A **32**, 251 (2007).
[4] V. I. Zagrebaev, Nucl. Phys. A **734**, 164 (2004).
[5] K. Siwek-Wilczynska, I. Skwira, and J. Wilczynski, Phys. Rev. C **72**, 034605 (2005).
[6] A. Yadav, V. R. Sharma, P. P. Singh, D. P. Singh, M. K. Sharma, U. Gupta, R. Kumar, B. P. Singh, R. Prasad, and R. K. Bhowmik, Phys. Rev. C **85**, 034614 (2012).
[7] A. Yadav, P. P. Singh, Mohd. Shuaib, V. R. Sharma, I. Bala, Unnati, S. Gupta, D. P. Singh, M. K. Sharma, R. Kumar, S. Murlithar, R. P. Singh, B. P. Singh, and R. Prasad, Phys. Rev. C **96**, 044614 (2017)
[8] Mohd. Shuaib, V. R. Sharma, A. Yadav, M. K. Sharma, P. P. Singh, D. P. Singh, R. Kumar, R. P. Singh, S. Muralithar, B. P. Singh, and R. Prasad, J. Phys. G: Nucl. Part. Phys. **44**, 105108 (2017).
[9] Mohd. Shuaib, V. R. Sharma, A. Yadav, P. P. Singh, M. K. Sharma, D. P. Singh, R. Kumar, R. P. Singh, S. Muralithar, B. P. Singh, and R. Prasad, Phys. Rev. C **94**, 014613 (2016).
[10] Mohd. Shuaib, V. R. Sharma, A. Yadav, M. K. Sharma, P. P. Singh, D. P. Singh, R. Kumar, R. P. Singh, S. Muralithar, B. P. Singh, and R. Prasad, Phys. Rev. C **98**, 014605 (2018).
[11] M. Shariq Asnain, Mohd. Shuaib, Ishfaq Majeed, M. K. Sharma, V. R. Sharma, A. Yadav, D. P. Singh, P. P. Singh, U. Gupta, R. N. Sahoo, A. Sood, M. Kaushik, S. Kumar, R. Kumar, B. P. Singh, and R. Prasad, Phys. Rev. C **104**, 034616 (2021).
[12] M. k. Sharma, B. P. Singh, S. Gupta, M. M. Musthafa, H. D. Bhardwaj, R. Prasad, and A. K. Sinha, J. Phys. Soc. Jpn. **72**, 1917 (2003).
[13] I. Tserruya, V. Steiner, Z. Fraenkel, P. Jackobs, D. G. Kovar, W. Henning, M. F. Vineyard, and B. G. Glagola, Phys. Rev. Lett. **60**, 14 (1988).
[14] M. K. Sharma, M. M. Musthafa, Mohd Shuaib, M. Kumar, V. R. Sharma, A. Yadav, P. P. Singh, B. P. Singh, and R. Prasad, Phys. Rev. C **99**, 014608 (2019).
[15] M. K. Sharma, M. Sarswat, S. Arora, S. Kumar, Mohd. Shuaib, Ishfaq Majeed, M. Shariq Asnain, V. R. Sharma, A. Yadav, P. P. Singh, D. P. Singh, B. P. Singh, and R. Prasad, Phys. Rev. C **104**, L031601 (2021).
[16] L. F. Canto, P. R. S. Gomes, R. Donangelo, and M. S. Hussein, Phys. Rep. **424**, 1 (2006).
[17] N. Keeley, R. Raabe, N. Alamanos, and J. Sida, Prog. Part. Nucl. Phys. **59**, 579 (2007).
[18] B. B. Back, H. Esbensen, C. L. Jiang, and K. E. rehm, Rev. Mod. Phys. **86**, 317 (2014).
[19] L. F. Canto, P. R. S. Gomes, J. Lubian, L. C. Chamon, and E. Crema, Nucl. Phys. A **821**, 51 (2009) and references therein.
[20] P. R. S. Gomes, L. F. Canto, L. Lubian, P. Lotti, L. C. Chamon, E. Crema, and J. M. B. Shorto, Nucl. Phys. A **834**, 151c (2010).
[21] M. Beckerman, M. Salomaa, A. Sperduto, J. D. Molitoris, and A. DiRienzo, Phys. Rev. C **25**, 837 (1982).
[22] P. R. S. Gomes, J. Lubian, I. Padron, and R. M. Anjos, Phys. Rev. C **71**, 017601 (2005).
[23] L. F. Canto, P. R. S. Gomes, J. Lubian, L. C. Chamon, and E. Crema, J. Phys. G: Nucl. Part. Phys. **36**, 015109 (2009).
[24] R. Wolski, Phys. Rev. C **88**, 041603(R) (2013).
[25] M. Dasgupta, P. R. S. Gomes, D. J. Hinde, S. B. Moraes, R. M. Anjos, A. C. Berriman, R. D. Butt, N. Carlin, J. Lubian, C. R. Morton, J. O. Newton, and A. Szanto de Toledo, Phys. Rev. C **70**, 024606 (2004).
[26] P. K. Rath, S. Santra, N. L. Singh, R. Tripathi, V. V. Parkar, B. K. Nayak, K. Mahata, R. Palit, S. Kumar, S. Mukherjee, S. Appannababu, and R. K. Choudhury, Phys. Rev. C **79**, 051601(R) (2009).
[27] H. Kumawat, V. Jha, V. V. Parkar, B. J. Roy, S. K. Pandit, R. Palit, P. K. Rath, C. S. Palshetkar, S. K. Sharma, S. Thakur, A. K. Mohanty, A. Chatterjee, and S. Kailas, Phys. Rev. C **86**, 024607 (2012).
[28] V. Tripathi, A. Navin, K. Mahata, K. Ramachandran, A. Chatterjee, and S. Kailas, Phys. Lett. **88**, 172701 (2002).
[29] V. Tripathi, A. Navin, V. Nanal, R. G. Pillay, K. Mahata, K. Ramachandran, A. Shrivastava, A. Chatterjee, and S. Kailas, Phys. Rev. C **72**, 017601 (2005).
[30] L. R. Gasques, D. J. Hinde, M. Dasgupta, A. Mukherjee, and R. G. Thomas, Phys. Rev. C **79**, 034605 (2009).
[31] K. Kalita, J. Phys. G: Nucl. Part. Phys. **38**, 095104 (2011).
[32] M. Dasgupta, L. R. Gasques, D. H. Luong, R. du Rietz, R. Rafiei, D. J. Hinde, C. J. Lin, M. Evers, and A. Diaz-Torres, Nucl. Phys. A **834**, 147c (2010).
[33] V. V. Sargsyan, G. G. Adamian, N. V. Antonenko, W. Scheid, and H. Q. Zhang, Phys. Rev. C **86**, 054610 (2012).
[34] P. R. S. Gomes, R. Linares, J. Lubian, C. C. Lopes, E. N. Cardozo, B. H. F. Pereira, and I. Padron, Phys. Rev. C **84**, 014615 (2011).
[35] P. K. Rath, S. Santra, N. L. Singh, K. Mahata, R. Palit, B. K. Nayak, K. Ramachandran, V. V. Parkar, R. Tripathi, S. K. Pandit, S. Appannababu, N. N. Deshmukh, R. K. Choudhury, and S. Kailas, Nucl. Phys. A **874**, 14 (2012).
[36] M. K. Pradhan, A. Mukherjee, P. Basu, A. Goswami, R. Kshetri, Subinit Roy, P. Roy Chowdhury, M. Saha Sarkar, R. Palit, V. V. Parkar, S. Santra, and M. Ray, Phys. Rev. C **83**, 064606 (2011).
[37] C. S. Palshetkar, S. Thakur, V. Nanal, A. Shrivastava, N. Dokania, V. Singh, V. V. Parkar, P. C. Rout, R. Palit, R. G. Pillay, S. Bhattacharyya, A. Chatterjee, S. Santra, K. Ramachandran, and N. L. Singh, Phys. Rev. C **89**, 024607 (2014).

[38] P. K. Rath, S. Santra, N. L. Singh, B. K. Nayak, K. Mahata, R. Palit, K. Ramachandran, S. K. Pandit, A. Parihari, A. Pal, S. Appannababu, S. K. Sharma, D. Patel, and S. Kailas, Phys. Rev. C **88**, 044617 (2013).
[39] A. Gavron, Phys. Rev. C **21**, 230 (1980).
[40] M. Beckerman, Rep. Prog. Phys. **51**, 1047 (1988).
[41] M. Beckerman, Phys. Rep. **129**, 145 (1985).
[42] K. Hagino, N. Rowley, and A. T. Kruppa, Comput. Phys. Commun. **123**, 143 (1999).
[43] K. Hagino, N. Takigawa, A. B. Balantekin, and J. R. Bennett, Phys. Rev. C **52**, 286 (1995).
[44] N. Austern, Y. Iseri, M. Kamimura, M. Kawai, G. Rawitscher, and M. Yahiro, Phys. Rep. **154**, 125 (1987).
[45] R. Linares, M. Sinha, E. N. Cardozo, V. Guimarães, G. V. Rogachev, J. Hooker, E. Koshchiy, T. Ahn, C. Hunt, H. Jayatissa, S. Upadhyayula, B. Roeder, A. Saastomoinen, J. Lubian, M. Rodríguez-Gallardo, J. Casal, K. C. C. Pires, M. Assunção, Y. Penionzhkevich, and S. Lukyanov, Phys. Rev. C **103**, 044613 (2021).
[46] A. Gómez Camacho, JPS Conf. Proc. **32**, 010011 (2020)
[47] M. A. G. Alvarez, M. Rodriguez-Gallardo, J. P. Fernandez-Garcia, J. Casal, and J. A. Lay, Phys. Rev. C **103**, 054614 (2021).
[48] C. Beck, N. Keeley, and A. Diaz-Torres, Phys. Rev. C **75**, 054605 (2007).
[49] K. Zerva, N. Patronis, A. Pakou, N. Alamanos, X. Aslanoglou, D. Filipescu, T. Glodariu, M. Kokkoris, M. La Commara, A. Lagoyannis, M. Mazzocco, N. G. Nicolis, D. Pierroutsakou, M. Romoli, and K. Rusek, Phys. Rev. C **80**, 017601 (2009).
[50] K. Wang, Y. Y. Yang, A. M. Moro, V. Guimarães, Jin Lei, D. Y. Pang, F. F. Duan, J. L. Lou, J. C. Zamora, J. S. Wang, Z. Y. Sun, H. J. Ong, X. Liu, S. W. Xu, J. B. Ma, P. Ma, Z. Bai, Q. Hu, X. X. Xu, Z. H. Gao, G. Yang *et al.*, Phys. Rev. C **103**, 024606 (2021).
[51] http://nrv.jinr.ru/nrv/webnrv/fusion/.
[52] C. Y. Wong, Phys. Rev. Lett. **31**, 766 (1973).
[53] P. P. Singh, A. Yadav, V. R. Sharma, R. Kumar, M. K. Sharma, B. P. Singh, R. P. Singh, S. Muralithar, R. K. Bhowmik, and R. Prasad, J. Phys.: Conf. Ser. **590**, 012031 (2015).
[54] V. R. Sharma, A. Yadav, P. P. Singh, D. P. Singh, S. Gupta, M. K. Sharma, I. Bala, R. Kumar, S. Murlithar, B. P. Singh, and R. Prasad, Phys. Rev. C **89**, 024608 (2014).
[55] P. P. Singh, B. P. Singh, M. K. Sharma, Unnati, D. P. Singh, R. Prasad, R. Kumar, and K. S. Golda, Phys. Rev. C **77**, 014607 (2008).
[56] P. P. Singh, M. K. Sharma, Unnati, D. P. Singh, R. Kumar, K. S. Golda, B. P. Singh, and R. Prasad, Eur. Phys. J. A **34**, 29 (2007).
[57] B. Wang, W.-J. Zhao, P. R. S. Gomes, E.-G. Zhao, and S.-G. Zhou, Phys. Rev. C **90**, 034612 (2014).